Reactive Wetting of an Iron-Base Superalloy MSA2020 and 316L Stainless Steel by Molten Zinc-Aluminum Alloy

JING XU, XINGBO LIU, MARK A. BRIGHT, JAMES G. HEMRICK, VINOD SIKKA, and EVER BARBERO

The reactive wetting behaviors of MSA2020, an Fe-based superalloy, and 316L stainless steel in contact with a molten Zn-Al alloy were investigated by the sessile drop method. This investigation led to the following findings. (1) 316L not only suffered considerable wetting, but also reacted with the molten Zn-Al alloy at a higher rate than MSA2020. (2) The contact angle of MSA2020 wet by the molten Zn-Al alloy dropped to an acute angle when the temperature was increased to 500 °C. (3) The surface reaction was found to initiate even though the liquid droplet and substrate were observed as nonwetting (contact angle larger than 90 deg). (4) The reaction mechanisms were identified in three stages. Initially, the Al diffused into the substrate to form an Fe-aluminide layer, which acted as the reaction front. Next, the reaction front penetrated the substrate through inward diffusion of Al. Finally, Zn-rich zones formed behind the reaction front as a result of Al depletion. (5) The alloying constituents (W, Mo, and Cr) in MSA2020 stably segregating on the surface reduced the wettability by molten Zn-Al by covering the reactive sites on the solid-liquid interface.

DOI: 10.1007/s11661-008-9501-x
© The Minerals, Metals & Materials Society and ASM International 2008

I. INTRODUCTION

CORROSION and erosion of pot hardware by molten Zn-Al alloy have long been an issue of concern in the galvanizing processing industry.[1–6] The formation of intermetallic phases by reaction between the metallic hardware and galvanizing media would aggravate the dross buildup on the pot rolls and bearings and, thus, reduce the service life of the pot hardware. Frequent line stoppages for maintenance are required to avoid impairment to the coating quality as a result of excessive dross formation. Therefore, extensive research efforts have been conducted to examine the reaction of molten Zn-Al alloy baths with various materials, including ceramics, cermet, steel, and superalloys.[7]

The wettability of solids by liquid metals at high temperature carries important implications of interfacial reaction mechanisms for liquid/solid contact.[8] The reactive wetting behaviors of steels in molten Zn-Al baths have been well examined by attempts to evaluate the effectiveness of the galvanizing processes. In particular, it was found by Brondyke that progressive wetting and subsequent penetration of Al-Si carbide materials by molten Al at 700 °C to 1000 °C gave rise to reactive product buildup and tensile stress formation.[9] As for galvanizing high-strength steel in molten Zn-Al alloy, a study by Bordignon indicated selective oxidation of segregated Mn and Si at 800 °C during annealing before hot dipping reduced wettability and reactivity of molten zinc and aluminum on free iron at 460 °C. Additionally, the presence of nonoxidizable constituents such as Sn and P improved wettability by reducing preferential oxidation.[10] Through a similar research project, Giorgi *et al.* further pointed out the variance of selective oxidation from segregated constituents as a result of inconsistencies in annealing time and temperature and the consequential impact on reactive wetting, as determined by sessile drop measurements.[11] Gradual improvement of the contact angle with time between a silicon-bearing steel and zinc at 470 °C has been observed by Chung *et al.*[12] The complete coverage of the steel surface by a zinc droplet 20 minutes after dipping indicates the rate-limiting reaction kinetics. In distinctive contrast, a dynamic-dominant wetting behavior has been found for dip coating of low-carbon steel with Al-Zn-Si alloy melts by Ebrill *et al.*[13] The contact angle displays an abrupt transition from nonwetting to wetting within 2 ms of the dipping process, a reduction of wetting angle from 125 to 25 deg as a result of preheating of the steel substrate up to the droplet melt temperature. Such an improvement of the wetting condition was also found to greatly facilitate the mass transfer of iron atoms from the substrate toward the melt, resulting in formation of alloy layer phases with high Fe content.

On the other hand, studies of the reaction of alloy materials with molten zinc-aluminum alloy have been carried out in terms of analysis of weight loss and dimensional changes.[14] In more recent work completed

JING XU, Graduate Research Assistant, XINGBO LIU, Assistant Professor, and EVER BARBERO, Professor, are with the Mechanical & Aerospace Engineering Department, West Virginia University, Morgantown, WV 26506. Contact e-mail: xingbo.liu@mail.wvu.edu MARK A. BRIGHT, Technology Manager, is with the Metallics Systems (Division of Pyrotek Incorporated), Solon, OH 44139. JAMES G. HEMRICK, Staff Member, and VINOD SIKKA, Manager, are with the Materials Science & Technology Division, Oak Ridge National Laboratory, Oak Ridge, TN 37831.

Manuscript submitted August 29, 2007.
Article published online April 2, 2008

on Co- and Fe-based superalloys, Zhang *et al.* investigated the corrosion process by examining reaction kinetics and product evolution.[1,4] It was found in their work that the attack of Zn-Al bath on the superalloys initiated with the formation of Fe-aluminide or Co-aluminide on the surface followed by inward propagation of a reaction front and the subsequent buildup of dross particles on the top of the residual zinc-rich reaction zone formed on the aluminide layer. However, few reports have previously identified the initial development of the reaction characteristics of superalloys in terms of reactive wetting, which is important in understanding the reactivity of superalloys during actual service conditions. Hence, a need exists for an in-depth investigation on the incipient liquid/solid contact stage by molten zinc through a detailed wetting study.

In this article, work was described on a comparative study of reactive wetting behaviors between 316L stainless steel and an Fe-based superalloy, MSA2020 with molten zinc bath. The initiation of the reaction process and the reactivity of these materials were examined by analyzing contact angles and droplet geometry. Evolution of the liquid/solid reaction was further explored by conducting compositional and structural analysis on the interfacial reaction layers. The formed intermetallic resultant compounds were studied by both electron probe microanalysis (EPMA) and energy-dispersive spectroscopy (EDS) analysis. Reactive wetting theories were employed to support the analysis of the sessile drop test results. The results provide fundamental insight into the understanding of the reaction mechanisms of superalloy materials in a molten zinc bath and facilitate optimization and application of Fe-based superalloy MSA2020 as a pot hardware material in the galvanizing industry.

II. EXPERIMENTAL

A. *Materials*

The 316L stainless steel and MSA2020 (the Fe-based, carbide-rich superalloy supplied by the Metaullics Systems Division, Pyrotek Inc.) were studied as the substrate materials in this wetting investigation (Table I). The as-cast MSA2020 contained a continuous microscopic network of interpenetrating microscopic intermetallic phases and solid solution metallic phases. The presence of metallic phases provided significant improvement in toughness and damage tolerance, while the intermetallic phases contributed to high hardness and improved performance at elevated temperatures. The microstructures of the substrates, MSA2020 superalloy and 316L stainless steel, are shown in Figures 1(a) and (b), respectively. As can be seen in Figure 1(a), MSA2020 consisted of distinct primary dendrites of a Mo/W-containing intermetallic phase as well as a Cr-enriched intermetallic phase bound together with a network of eutectic solid solution phase matrix.

Galvanizing zinc alloy, which contained 0.23 wt pct Al, was machined down to cubes (5 mm × 5 mm × 3 mm) for melting during static wetting tests and also extruded into wire segments of 3-mm diameter in order to produce molten sessile drops during dynamic testing. Substrate

Table I. Chemical Composition of the Substrate Materials (Weight Percent)

Materials	C	Si	Mn	S	P	Cr	Ni	Mo	Co	W	B	Ta	Cu	N	Fe
316L ss	0.012	0.40	1.39	0.029	0.024	17.55	10.74	2.05	—	—	—	—	0.257	0.051	67.5

MSA 2020 a proprietary iron-based superalloy containing primary alloying additives of Cr, Co, Mo, Ni, and W.

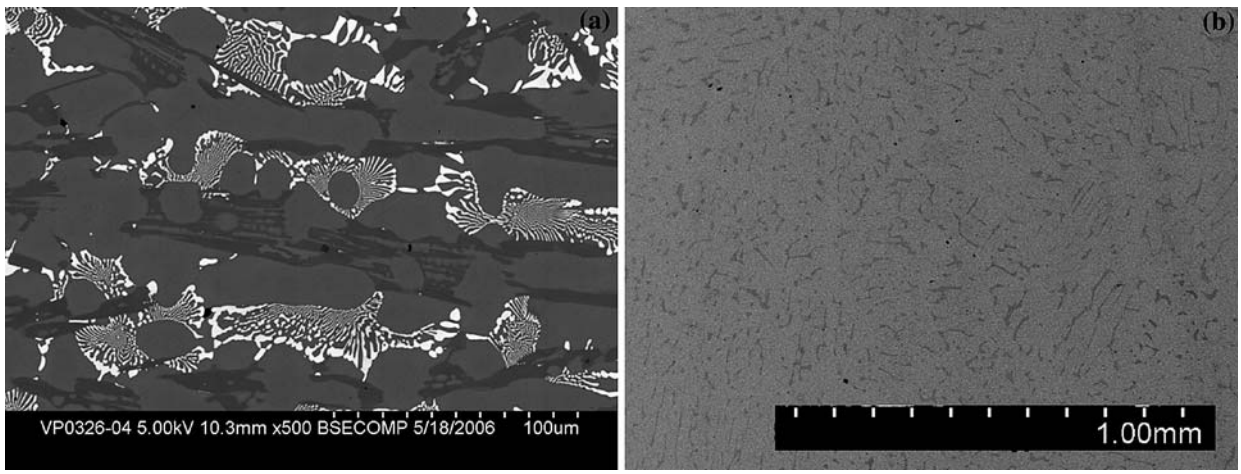

Fig. 1—Microstructure of the tested samples: (*a*) MSA2020 and (*b*) 316L.

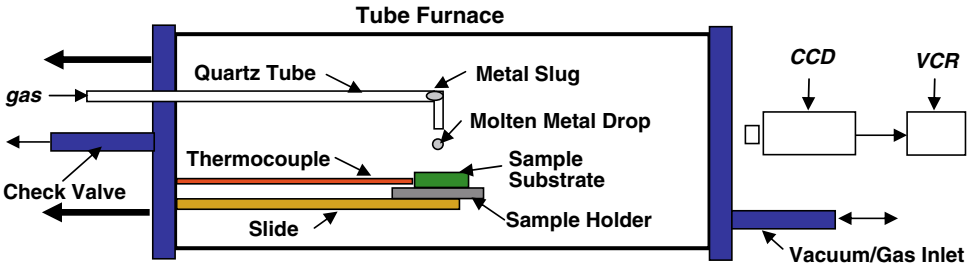

Fig. 2—Schematic sketch of the sessile drop unit.

samples (316L stainless steel and MSA2020 superalloy) were cut (12 mm × 12 mm × 3 mm) from originally supplied materials. Experiments were carried out in purified Ar-4 pct H_2 at various temperatures from 465 °C to 500 °C and different testing durations from 1 to 4 hours. The changes in contact angle between the molten Zn alloy and the substrates were monitored over time using a high-speed charge-coupled device (CCD) camera.

B. *Experiments*

Both static and dynamic sessile drop methods were employed for studying the wettability. According to the static method (which is the most conventional method), a solid cube of metal is placed on a substrate prior to heating. A modified dynamic method was also employed in which molten zinc alloy was dropped on the substrate by a heated delivery device. This modified method was developed to more effectively study the dynamic wetting behavior, as this approach has been suggested to be closer to the application conditions.[15] The apparatus used for both methods of sessile drop experiments is schematically illustrated in Figure 2, and it consists of a 33 kW horizontal circular IR furnace fitted with a rotary pump evacuating system and continuous gas system supplying purified Ar-4 pct H_2. The quartz furnace chamber was enclosed on one end by a copper lid and slide device, which was used to move the experimental assembly inside the chamber. A small diameter quartz tube was also passed through the copper lid and extended to a location directly above the sample substrate where the tube was bent 90 deg and its diameter was reduced. This tube was used to contain the zinc alloy wire segment during heating and melting, which produced the molten metal drop for the dynamic tests. Both sealed end caps of the furnace assembly contained quartz windows, allowing a high-resolution color CCD camera to continuously monitor the experiments. Three type-S thermocouples (with ceramic sheath) were inserted into the horizontal quartz test chamber through the copper end plate for monitoring of the substrate temperature, molten metal drop temperature, and the reaction temperatures.

Before each experiment, the substrate and the zinc alloy cube (or wire segment) were ultrasonically cleaned in acetone and the substrate was then carefully slid into the center of the horizontal chamber. For the static sessile drop method, a cube of zinc alloy was placed on top of the substrate prior to heating. The sealed chamber was evacuated to a vacuum of 1×10^{-6} Pa and then refilled with the purified Ar-4 pct H_2 gas. Following gas purging, the infrared (IR) quartz chamber was heated to the required temperature at a rate of 30 °C per minute. The cube of metal was allowed to melt and the wetting behavior between the zinc alloy and the substrate was observed.

For the dynamic sessile drop method, a wire segment of zinc alloy was placed into the quartz tube used for delivering molten zinc to the substrate, and this tube was inserted through the copper end plate into the IR chamber. The chamber was evacuated and refilled, in the same manner as for the static test. While the zinc segment in the quartz tube was kept at the cold zone, the IR quartz chamber was heated to the required temperature at a rate of 30 °C per minute. The furnace was allowed to stabilize for 20 minutes before the zinc segment was slowly moved from the cold zone to the hot zone of the furnace, where it was allowed to melt and pass through the vertical portion of the delivery tube as a molten drop onto the test substrate. Similar to the static test method, the entire duration of the experiment was captured and recorded by the camera, from which video still frames were extracted and analyzed.

At the end of each experiment, the substrate was removed from the furnace and prepared for examination. Metallographic specimens of the as-received materials and cross sections of the tested samples were prepared following a standard procedure. The identification of reaction products was conducted using a JEOL* 8200 EPMA with details of the reaction products in the samples examined using a Hitachi 4700 scanning electron microscope (Pleasanton, CA) equipped with an integral EDS. Also, the depths of the reaction layers were measured using image analysis software (Image-Pro Plus 4.0, Media Cybernetics, Bethesda, MD).

*JEOL is a trademark of Japan Electron Optics Ltd., Tokyo.

III. RESULTS

A. *Wetting and Contact Angle*

Sessile drop testing is a powerful tool for the study of the transient stages of initial solid-liquid contact and its subsequent evolution, which is a result of the

minimization of interfacial energy. Hence, contact angle and drop dimensional observations, as well as the interfacial characterization, were reviewed for two substrate alloy and molten zinc systems.

Illustrating the changes in contact angle and drop geometry with time, Figure 3 shows images of a molten zinc drop on the 316L stainless and MSA2020 substrates during isothermal dwelling at 485 °C. The initial contact angle between the 316L substrate and liquid zinc alloy was an obtuse angle (> 90 deg) (Figure 3(b)), but was found to gradually decrease to an acute angle (< 90°) during a hold time of 30 minutes, indicative of the occurrence of reactive wetting (Figure 3(c)). After the dwelling time was extended to 60 minutes, approximately 50 pct of the molten zinc alloy diffused into the 316L base, significantly changing the geometry of the zinc droplet. At the end of the test (after 120 minutes), almost all the molten zinc permeated into the 316L substrate by diffusion and chemical reaction (Figure 3(d)). Conversely, the contact angle on the MSA2020 superalloy remained at an obtuse angle throughout the entire 120 minutes dwell time. This final state was considered to represent the obtaining of reactive wetting equilibrium. Differences on the wetting performance between the 316L stainless and MSA2020 base materials are potentially due to the variance in the microstructure and chemical composition of the substrates, leading to the divergence of the reactive wetting kinetics.

Four parameters, namely, contact angle (CA), drop volume (V), drop base diameter (D), and drop height (H), were analyzed to gain insight into the reactive wetting kinetics. The wetting kinetics could be inferred by combination of the changes in contact angle with the changes in drop size. The change in contact angle characterized by the advance of the triple phase reaction (that where the solid substrate, liquid metal, and gaseous experimental environment are in contact) was due to the decrease in the drop height or the increase in the drop base diameter. The determinant factor depended on the specific wetting system. From Figure 3, it was observed that the drop volume of both 316L stainless and MSA2020 continuously decreased during the wetting process, minimizing the drop volume present at the end of the wetting tests after 120 minutes. Combining the results obtained after 2 hours at both 465 °C and 485 °C, shown in Figure 3(d) with Figure 4(a), respectively, it was found that the decrease of the drop height was the dominant substage for the wetting of MSA2020, while the increase in drop base

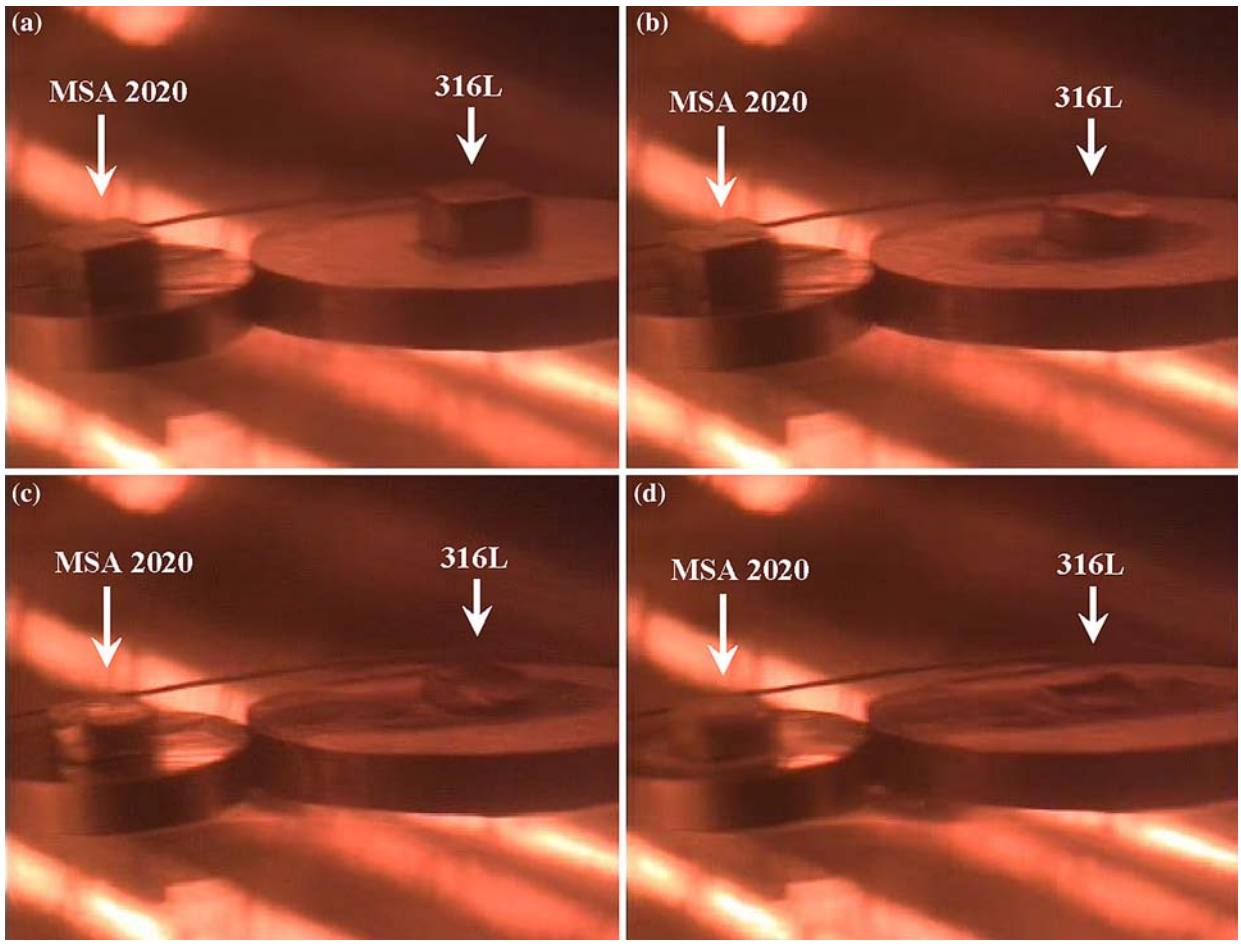

Fig. 3—Wetting of MSA2020 (left) and 316L stainless steel (right) with the Zn-0.23Al droplet at 485 °C: (*a*) initial stage, (*b*) after 10 min, (*c*) after 30 min, and (*d*) after 120 min.

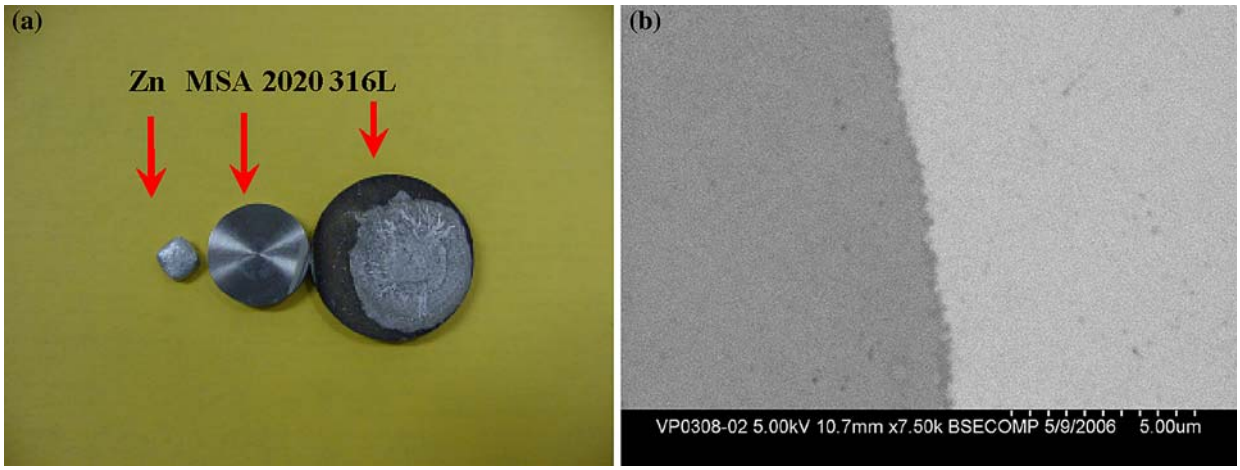

Fig. 4—Wetting with the Zn-0.23Al droplet at 465 °C after 2 h: (*a*) MSA2020 optical microscopic view and (*b*) 316L stainless steel backscattered micrograph.

diameter by spreading of the molten zinc overwhelmed the reactive wetting process on 316L stainless.

At 465 °C, molten zinc did not wet the MSA2020 after 2 hours, as evident by the solidified drop easily detaching from the substrate after the test without any adhesion (Figure 4(a)). However, when the dwelling time was extended from 2 to 4 hours at 465 °C, the molten zinc drop could stick onto the MSA2020 surface more readily, although the contact angle was as large as 145 °C (Figure 5(c)). The EPMA analysis showed that a thin Fe-aluminide layer was formed, bonding with the MSA2020 substrate (Figures 5(d) through (h)). Increasing the heating temperature from 465 °C to 485 °C and subsequently to 500 °C, the wetting performance of MSA2020 was studied at higher temperatures. A small molten zinc "pond" was observed around the drop at 485 °C, indicating the increase of the drop base diameter (Figure 3(d)). Analyzing the cross-sectional interface, the contact angle was found to be greater than 90 deg (Figure 6(a)) despite initiation of reactive wetting and formation of reaction products in the substrate-liquid drop interface (Figure 6(b)). Additionally, a tiny crack was found at the edge of the droplet (Figure 6(a)), probably caused by the coefficient of thermal expansion mismatch between zinc and the MSA2020 substrate during cooling. It is hypothesized that the temperature enhancement may decrease the contact angle as a result of enlargement of the droplet on the substrate from greater molten metal fluidity. As an example, the 500 °C sessile drop results showed that the contact angle of MSA2020 was reduced to less than 90 deg (Figure 7(a)), and an interfacial Fe-aluminide intermetallic layer was also observed under such an experimental condition (Figure 7(b)).

On the other hand, for the 316L substrate, the molten zinc spread over the base surface (Figure 4(a)) and the droplet height decreased to nearly zero in all the experiments regardless of the heating temperature (465 °C, 485 °C, and 500 °C) or dwelling time (1, 2, and 4 hours). The Fe-aluminide reaction layer was detected by EPMA with varying thickness from the cross-sectional microstructures, as shown in Figures 4(b), 5(b), 6(d), and 7(d). Furthermore, reviewing the droplet geometry and macrobonding, a comparison can be made on the wettability of the substrate, 316L and MSA2020, with molten Zn-0.23 wt pct Al alloy. As observed in Figures 5(a) and (c), for 465 °C-4 hours wetting tests, and in Figures 6(a) and (c), for 485 °C-2 hours wetting test, the contact angle of MSA2020 remained obtuse while 316L displayed an acute angle at the above two testing conditions. Conversely, it was determined that 500 °C facilitated the wetting activity for both 316L and MSA2020 by reducing the contact angle below 90 °C, as shown in Figures 7(a) and (c).

It must also be noted that the substrate corrosion reaction could take place even though the contact angle is larger than 90 °C. Conventionally, the contact angle is used to differentiate wetting from nonwetting and a contact angle of 90 deg or greater generally characterizes a surface as nonwetting. However, this concept is deduced from the macro point of view. Experimental interpretation indicated that the metallurgical reaction may occur even when the liquid droplet and substrate were observed as nonwetting (contact angle is larger than 90 deg).

B. *Interfacial Morphology Examination of Reaction Layers*

The reaction of 316L and MSA2020 with the Al-containing Zn alloy was found to initiate with the formation of Fe-aluminide layers, regardless of the temperature (ranging 465 °C from to 500 °C) or time (ranging from 1 to 4 hours), and a continuous Fe-aluminide layer was distinctive in both 316L and MSA2020. These Fe-aluminide layers were most likely based on a Fe_2Al_5 structure[16–18] with some of the Fe sites substituted by Cr, Si, and Mo atoms. The δ phase with diffused Al was also identified as a reaction zone in 316L and MSA2020 in a region receding the Fe-aluminide front layer. The boundaries between the different phases of wetting for MSA2020 were very clear

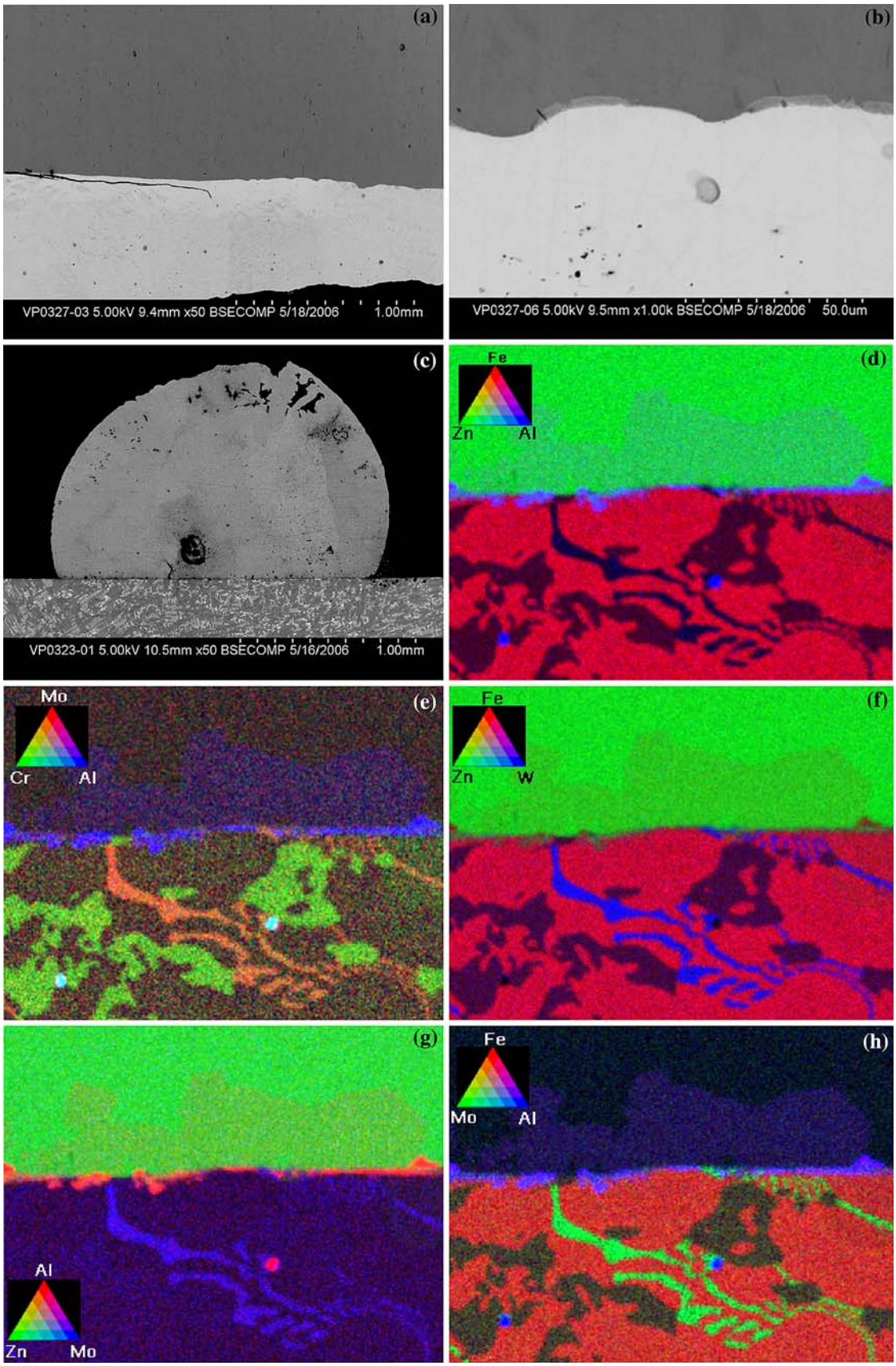

Fig. 5—Backscattered micrographs and electron microprobe mapping of wetting with the Zn-0.23Al droplet at 465 °C after 4 h: (*a*) and (*b*) BSE of 316L stainless steel, (*c*) BSE of MSA2020, and (*d*) through (*h*) EPMA of MSA2020 superalloy.

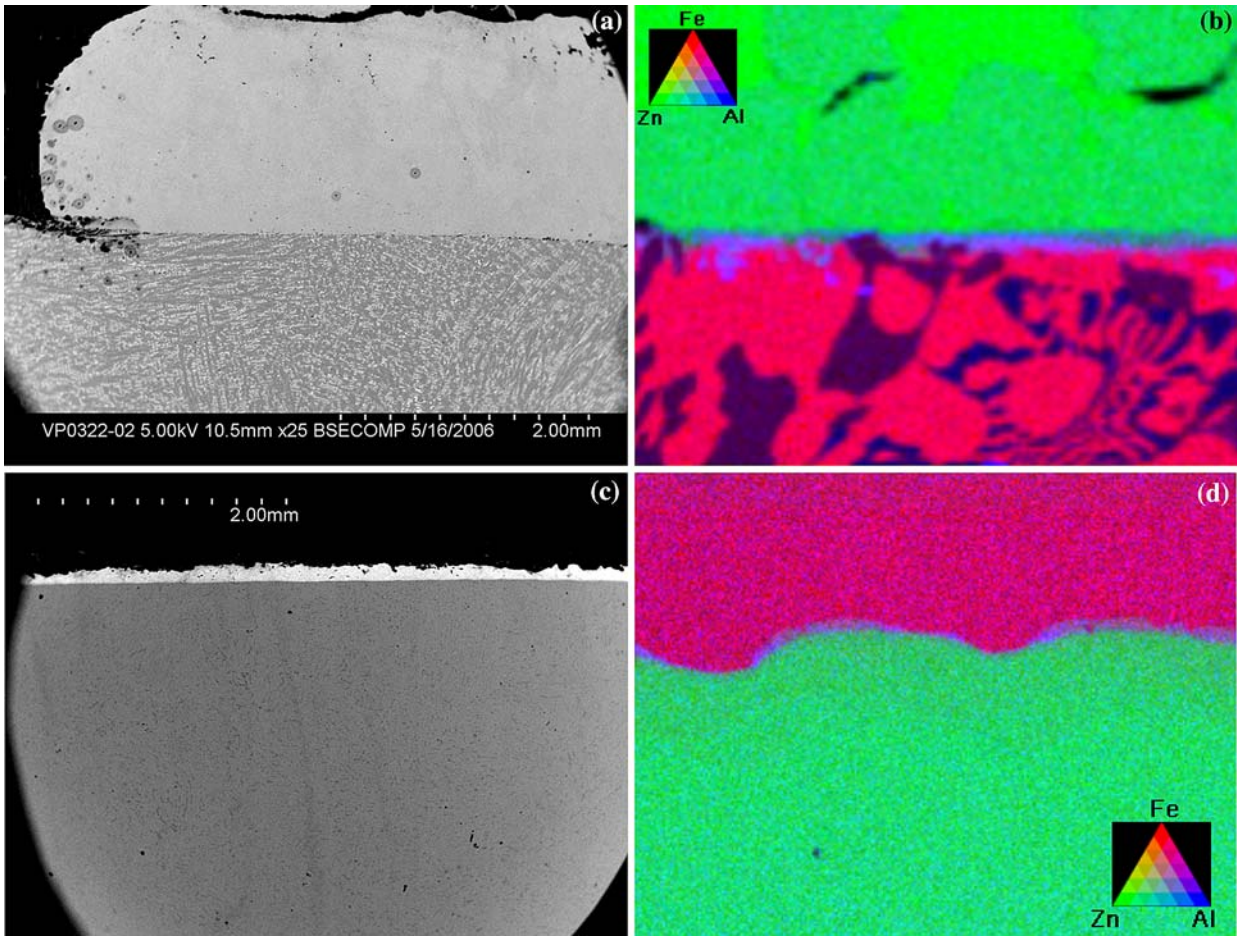

Fig. 6—Backscattered micrographs and electron microprobe mapping of MSA2020 wetting with the Zn-0.23Al droplet after 2 h at 485 °C: (*a*) BSE of MSA2020, (*b*) EPMA of MSA2020, (*c*) BSE of 316L stainless steel, and (*d*) EPMA of 316L stainless steel.

in the EMPA mappings. However, since the molten zinc alloy has a strong affinity for 316L stainless, most molten zinc either penetrated down to the 316L base or flowed over the contact surface, leading to only a very small amount of zinc remaining on the 316L surface. With a minimal amount of residual zinc thickness, it was difficult to detect the boundary between the δ phase and the zinc alloy matrix.

As the wetting time at 465 °C increased from 2 hours (Figure 4) to 4 hours (Figure 5), the reaction front in the form of an aluminide layer moved further inward from the sample surface and a Zn-rich zone was left behind. As a result, the thicknesses of the reaction layers increased from 0.2 μm (Figures 4(b)) to 3 μm (Figures 5(b)). Similarly, the increase of the wetting temperature from 465 °C to 485 °C with the same dwelling time (2 hours) also facilitated the growth of the reaction layer from 0.2 μm (Figures 4(b)) to 5 μm (Figures 6(d)). Comparing with the two substrates under the same testing condition, such as 485 °C after 2 hours (Figures 6), the thickness of the reactive layer for 316L stainless (5 μm) was more than double that for MSA2020 (2 μm), indicating that the reaction driving force of 316L was larger than that of MSA2020. The weaker reactivity of MSA2020 may be explained by its poor affinity to the molten Zn-Al alloy, resulting in a lower diffusion coefficient. In other words, the interfacial reaction force of Zn-Fe was larger than the reaction of Zn-W/Mo. Neither W nor Mo diffused from MSA2020 into the interface,[19–21] while Fe did. Figure 7 shows that the result of 500 °C-1 hour wetting was comparable with that at 485 °C-2 hours with MSA2020 developing a 2-μm-thick intermetallic layer and 316L forming a 5-μm layer.

IV. DISCUSSION

A. *Characters of Reactive Wetting*

The results obtained in this study indicate that 316L stainless and MSA2020 (Fe-based superalloy) react readily with molten Zn-Al alloy, but the characteristics of the reactions varied with the alloys and evolved with the reactive wetting times. The reaction layers were generally continuous and compact, and the growth of the layers was proportional with the wetting time. Previously, Zhang *et al.* studied the long time (168 hours) dipping performance of Co-based and Fe-based superalloys in a Zn-0.22 wt pct Al bath and found that the growth of the reaction layer followed a

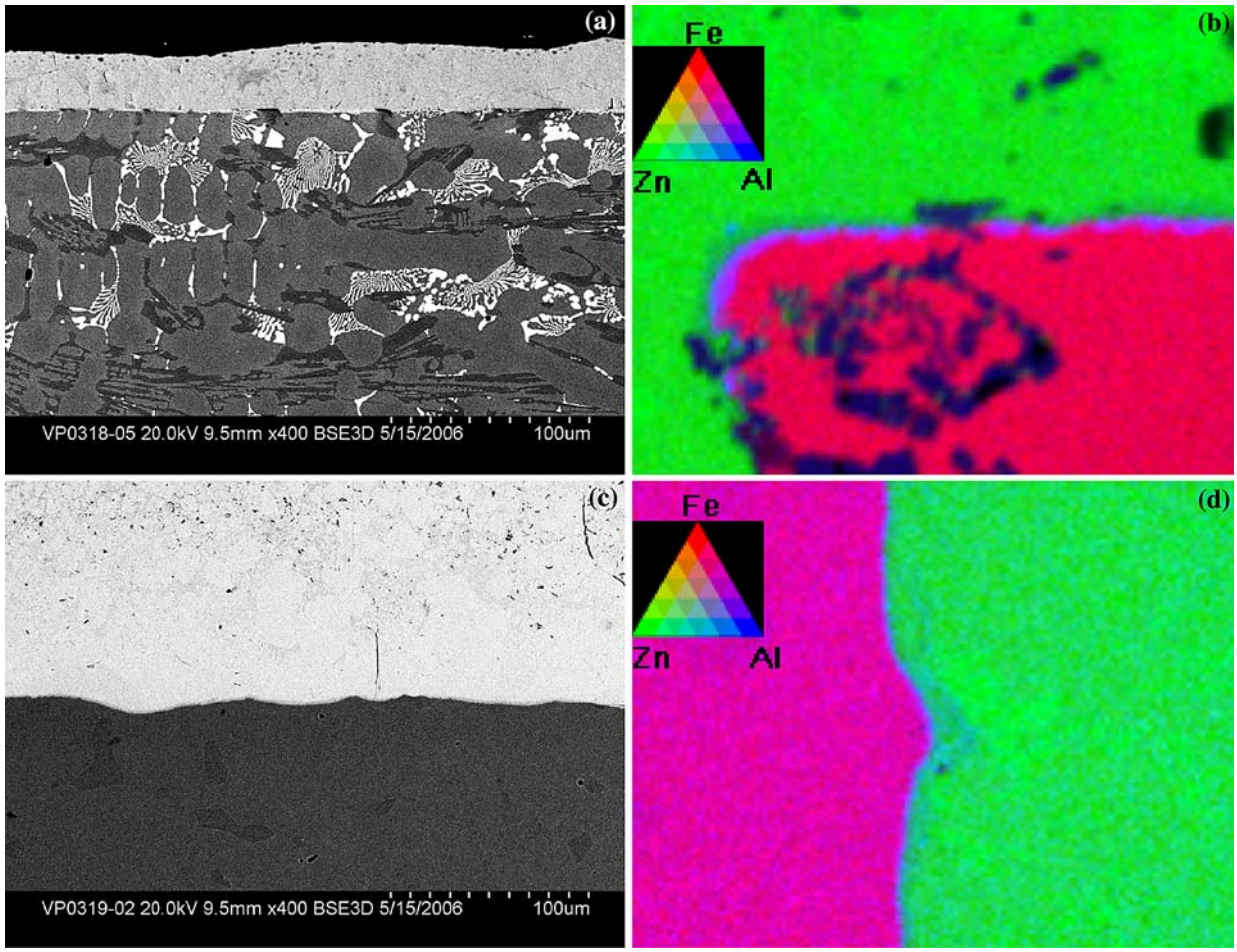

Fig. 7—Backscattered micrographs and electron microprobe mapping of MSA2020 wetting with the Zn-0.23Al droplet after 1 h at 500 °C: (*a*) BSE of MSA2020, (*b*) EPMA of MSA2020, (*c*) BSE of 316L stainless steel, and (*d*) EPMA of 316L stainless steel.

parabolic development,[1] indicating that the reactions were diffusion controlled. Hence, the reaction rates were determined by the diffusivity of the dominant reactant in the reaction layer. The findings in the current study imply that the reactive wetting behavior of MSA2020 superalloys in molten Zn-Al alloy is complicated in nature. In addition, the wetting tests prove that the reaction could happen even if the contact angle was observed to be obtuse. Thus, by simply measuring the dimensional or weight changes of the tested samples, the severity of the reaction of an alloy with the test media may be misinterpreted because the results of the measurements depend strongly on how the reaction products (consisting of the residual Zn overlay), the built-up layer, and the reaction layer are removed. Some researchers have judged the wettability of a material to molten alloy based only on the contact angle value,[22–23] and such discernment may significantly underestimate the extent of the reactive wetting because the reaction products may initiate development even with a contact angle larger than 90 deg. This discovery could, in part, explain discrepancies in the debate of wetting and reaction performance of results reported by different researchers on the materials in molten alloys.

To better understand the reactive wetting kinetics between the liquid zinc alloy and the substrate, it is necessary to discuss the reaction behaviors and the corresponding effects. The influence of the chemical reaction and formation of the Fe_2Al_5 intermetallic layer on the reactive wetting process is not clear. On one hand, the new phase formation promoted wetting of the substrate materials by the chemical reaction, which continuously consumed the reactive elements (Fe, Al, and Zn). The propagating chemical reaction assisted the reactive components at a high rate of diffusion, because the diffusion was driven by the concentration gradient. The accelerated diffusion facilitated the wetting and shortened the wetting time. On the other hand, the accumulation of the intermetallic compounds at the interface reduced the activity of the reactive wetting. It is perceived that the wettability also depends on the amount of active elements (*i.e.*, Fe) in the tested system. The new intermetallic phases (Fe_2Al_5) accumulated at the interface between the molten zinc alloy and the substrate partially covering the reactive sites and requiring the Fe to slowly diffuse across this aluminide layer. From this perspective, the Fe_2Al_5 reaction layer possessed effects similar to an inhibition layer, where

consumption of the Al by the Fe_2Al_5 intermetallic layer depleted the reactive Al at the substrate/zinc interface.

B. *Mechanism of Reactive Wetting*

The dimensional changes of the molten zinc droplet and increases of the reaction layers on the substrate were accompanied by a complicated phase evolution process. It was observed from EPMA mapping that Al is the most corrosive ingredient in the molten alloy, because it reacts with transition metals and forms aluminides with relatively low free energies of formation. The reaction of 316L stainless with the Zn-Al bath would obviously form Fe-aluminides (Fe_2Al_5 type) at the initial stages. A similar reaction took place in the case of MSA2020, but required longer time than 316L for inciting the reaction before the energy barrier was overcome.

The formation of the Zn-rich reaction zones behind the moving reaction fronts in the alloys created chemical compositions of the reaction zones that were quite different. The Zn-rich layer in the 316L contained close to 95 pct Zn and only 0.8 pct Al and is likely based on the δ-phase ($Zn_{10}M$). Conversely, the reaction zones formed in MSA2020 contained considerable amounts of Al (10.4 pct). In addition, EPMA mapping did not detect any Mo in the reaction zone, minimizing the likelihood of Mo-aluminide formation. This result differs from previous research on another Fe-based superalloy, T-500M, where a large amount of Mo_3Al_8 was found in the reaction zone.[4] This variance is possibly due to the difference in chemical composition of the solid solution phases in these alloys, where T-500M contained an appreciable amount of Mo while only a limited amount of Mo was added to MSA2020.

For both 316L stainless and MSA2020 superalloy, the reactive wetting could be explained in three steps. It started with the wetting and diffusion of the molten Zn-Al to the substrate, followed by the conversion of the Fe solid solution phase into an Fe-aluminide of the matrix components. Subsequently, this aluminide layer was converted into the δ phase ($Zn_{10}M$) in 316L and Zn-rich Al-Fe intermetallic phases in MSA2020. The relatively stable intermetallic phases containing Mo, W, and Cr were left undisturbed due to their dissension of molten zinc alloy. Apparently, such a three-step process allows the early participation of Zn in reactive wetting and, hence, is kinetically favored.

C. *Alloying Element Effects and Other Influence Factors*

It was concluded that the wettability was significantly affected by key factors such as alloying elements, the substrate density, and roughness of the substrate materials. For the MSA2020 superalloy, the alloying constituents segregating on the surface would cover part of the free iron surface and subsequently reduce wettability of molten zinc and aluminum with Fe. Moreover, introduction of Mo-W-Cr intermetallic phases at the solid-liquid interface offset the roughness effect on wetting, curving the interfacial boundary. The liquid zinc initially reacted with the Fe solid solution, which was located in the valley between those spattered intermetallic phases. The same conclusion was made in the case of Cu wetting by PbSn solder.[24,25] The difference in the roughness of the Cu_6Sn_5 intermetallic in the inner regions and at the reaction band at the edge of the solder imparted great effect on the wettability.

Moreover, the addition of alloying elements to the MSA2020 superalloys to promote the formation of Mo-W-Cr intermetallic phases apparently improved the resistance of the alloy to the reactive wetting by molten Zn-Al alloy. Results obtained in this study revealed that the phases containing Mo-W-Cr were more stable than the Fe solid solution phases, and these phases was not attacked by molten zinc alloy during the reactive wetting process. Containing Mo, W, and Cr of significant amount, MSA2020 displayed better wetting resistance than 316L, which contains Cr, Ni, and Mo. Further investigation is warranted to explore the mechanisms and to verify the applicability of MSA2020 superalloy as galvanizing pot hardware materials.

The surface roughness was another important factor influencing the wettability. Since all the specimens were polished under the same conditions, the effect caused by the surface roughness was assumed to be negligible compared with the interfacial reaction, which contributed more to the wetting dynamics. It is postulated that if the substrate materials were manufactured with a more porous structure, the substrate would adsorb the liquid phase, accelerating the wetting process. However, considering that the substrate, 316L stainless and MSA2020, were dense and compact, the decrease in contact angle was not a consequence of adsorption effects.

V. CONCLUSIONS

In order to explore the mechanism of reactive wetting occurring between zinc alloy and steel/superalloy substrates, the wetting behavior of a GI zinc alloy (Zn-0.23Al) was investigated using the sessile drop technique. A link can be made between the wettability and the activity for zinc and aluminum to react with metallic iron. It was found that Fe-aluminide, based on the Fe_2Al_5 phase, formed in the reaction layer on 316L stainless steel and MSA2020, an Fe-based superalloy. Alloying elements Mo/W/Cr added to the MSA2020 superalloy significantly improved the wetting resistance to molten zinc. Since the current reactive wetting theory suggested that the first intermetallic compound formed during the wetting reaction could influence the wetting properties, the reaction of the base alloy and molten zinc droplet was discussed. Several findings were observed.

1. MSA2020 superalloy possessed better wetting resistance than 316L in contact with the molten zinc alloy at test temperatures of 465 °C, 485 °C, and 500 °C. Less residual zinc was found on the surface of 316L than MSA2020 after the wetting tests, which lasted as long as 4 hours.
2. The contact angle of MSA2020 remained at an obtuse angle throughout the wetting tests of 4 hours at 465 °C and 2 hours at 485 °C. However, the

contact angle of MSA2020 wet by the molten zinc alloy dropped to an acute angle when the temperature was increased to 500 °C. Conversely, a molten zinc film started to spread over the 316L surface in the first half hour of dwelling at 465 °C. Reactive wetting became more severe when the temperature was increased.

3. The surface reaction was found to initiate even though the liquid droplet and substrate were observed as nonwetting (contact angle larger than 90 deg).
4. The reaction mechanisms were identified in three stages. Initially, the Al diffused into the substrate to form an Fe-aluminide layer, which acted as the reaction front. Next, the reaction front penetrated the substrate through inward diffusion of Al. Finally, Zn-rich zones formed behind the reaction front as a result of Al depletion.
5. The alloying constituents (W, Mo, and Cr) in MSA2020 stably segregating on the surface reduced the wettability by molten Zn-Al by covering the reactive sites on the solid-liquid interface.

ACKNOWLEDGMENTS

The authors thank the Metaullics Systems (Division of Pyrotek Inc.) for their cooperation to publish these results. Thanks are due to Wheeling-Nisshin, Inc. who helped with supplying the galvanizing zinc. We acknowledge the contributions of Randy Parton, Randy Howell, and Donny McInturff, ORNL, in support of the experimental execution described in this article. The efforts of Mingyang Gong in reviewing this document are also appreciated. This research was sponsored by the United States Department of Energy, Office of Energy Efficiency and Renewable Energy, Industrial Technologies Program, for the United States Department of Energy under Contract No. DE-FC36-04GO14038 and was supported by the Industries of the Future–West Virginia.

REFERENCES

1. K. Zhang and N.-Y. Tang: *Galvatech '04: 6th Int. Conf. on Zinc and Zinc Alloy Coated Steel Sheet—Conf. Proc.*, Chicago, IL, AIST, Warrendale, PA, 2004, pp. 617–27.
2. V. Parthasarathy, B.S.-J. Kang, A. Krishnaswamy, E. Barbero, K.M. Chang, C. Irwin, and F. Goodwin: *Galvatech '04: 6th Int. Conf. on Zinc and Zinc Alloy Coated Steel Sheet—Conf. Proc.*, Chicago, IL, AIST, Warrendale, PA, 2004, pp. 637–55.
3. W.J. Wang, J.P. Lin, Y.L. Wang, and G.L. Chen: *J. Univ. Sci. Technol.*, 2007, vol. 14, pp. 52–55.
4. K. Zhang and N.-Y. Tang: *Mater. Sci. Technol.*, 2004, vol. 20, pp. 739–46.
5. M.S. Brunnock, R.D. Jones, G.A. Jenkins, and D.T. Llewellyn: *Ironmaking and Steelmaking*, 1997, vol. 24, pp. 40–46.
6. M.S. Brunnock, R.D. Jones, G.A. Jenkins, and D.T. Llewellyn: *Ironmaking and Steelmaking*, 1996, vol. 23, pp. 171–76.
7. M.S. Brunnock, R.D. Jones, G.A. Jenkins, and D.T. Llewellyn: *Proc. Galvanizers Association*, Chicago, IL, 1996, pp. 3–15.
8. K. Nogi: *Proc. Result Presentations for International Joint Research Grant Program Proposals*, NEDO, 2005, p. H-17.
9. K. Brondyke: *J. Am. Ceram. Soc.*, 1953, vol. 36, pp. 171–74.
10. L. Bordignon: *ISIJ Int.*, 2001, vol. 41, pp. 168–74.
11. M.-L. Giorgi, M. Zaïdi, and J.-B. Guillot: *North American GAP Program Review Meeting*, Lexington, KY, ILZRO, Research Triangle, NC, 2005, p. 40.
12. Y. Chung, J. Wang, J.M. Toguri, and M.X. Yao: *Iron Steelmaker*, 2001, vol. 28, pp. 63–67.
13. N. Ebrill, Y. Durandet, and L. Strezov: *Metall. Mater. Trans. B*, 2000, vol. 31B, pp. 1069–79.
14. B. Gay, A. Piccinin, and M. Dubois: *Proc. Galvatech '01*, Brussels, 2001, pp. 262–69.
15. W. Fahrenholtz, K. Ewsuk, R. Loehman, and P. Lu: *J. Am. Ceram. Soc.*, 1998, vol. 81, pp. 2533–41.
16. X. Liu, E. Barbero, J. Xu, M. Burris, K.-M. Chang, and V. Sikka: *Metall. Mater. Trans. A*, 2005, vol. 36A, pp. 2049–58.
17. A.R. Marder: *Progr. Mater. Sci.*, 2000, vol. 45, pp. 191–271.
18. A.R.B. Verma and W.J. van Ooij: *Surf. Coat. Technol.*, 1997, vol. 89, pp. 132–42.
19. N. Tunca, G.W. Delamore, and R.W. Smith: *Metall. Trans. A*, 1990, vol. 21A, pp. 2919–28.
20. R. Eck: *Metall*, 1978, vol. 32, pp. 891–94.
21. J. Xu, M. Bright, X. Liu, and E. Barbero: *Metall. Mater. Trans. A*, 2007, vol. 38A, pp. 2727–36.
22. J.E. Kelley and H.M. Harris: *J. Test. Eval.*, 1974, vol. 2, p. 40.
23. A. Salehi, S. Tsai, V. Pawar, J. Sprague, G. Hunter, S. Varma, and F. Namavar: *Key Eng. Mater.*, 2006, vols. 309–311, pp. 1199–1202.
24. A.S. Zuruzi, C.-H. Chiu, S.K. Lahiri, and K.N. Tu: *J. Appl. Phys.*, 1999, vol. 86, pp. 4916–21.
25. A.J. Sunwoo, J.W. Morris, and G.K. Lucey: *Metall. Trans. A*, 1992, vol. 23A, pp. 1323–32.